Pergamon

PII: S1352-2310(97)00058-7

Atmospheric Environment Vol. 31, No. 19, pp. 3137-3150, 1997

1352-2310/97 $17.00 + 0.00

MODELLING OF RADIATION QUANTITIES AND PHOTOLYSIS FREQUENCIES IN THE AQUEOUS PHASE IN THE TROPOSPHERE

A. RUGGABER*,[1], R. DLUGI*, A. BOTT†, R. FORKEL‡, H. HERRMANN§ and H.-W. JACOBI§

*Ludwig-Maximilians-Universität München, Meteorologisches Institut, Theresienstr.37, D-80333 München, Germany; †Institut für Physik der Atmosphäre, Johannes Gutenberg Universität Mainz, Becherweg 21, D-55099 Mainz, Germany; ‡Fraunhofer Institut für Atmosphärische Umweltforschung, Kreuzeckbahnstr.19, D-82467 Garmisch-Partenkirchen, Germany and §Institut für Physikalische und Theoretische Chemie, Universität GH Essen, Universitätsstr. 5, D-45117 Essen, Germany

(*First received* 6 *March* 1996 *and in final form* 12 *December* 1996. *Published July* 1997)

Abstract—In order to provide information about photolysis frequencies in the aqueous phase for chemical transport models including wet chemistry a parameterization which can be added to gaseous-phase photolysis models was developed. The actinic fluxes inside cloud droplets are calculated on the basis of rigorous Mie theory taking into account the effect of dissolved particulate aerosol material and 10 representative cloud droplet size distributions. The results show that the actinic flux inside cloud droplets are on the average more than twice as large as compared to the interstitial air. The newly developed parameterization has been applied together with the model STAR (System for Transfer of Atmospheric Radiation). Apart from the parameters influencing gas-phase photolysis frequencies the radiation quantities inside the cloud droplets and therefore the photolysis frequencies in the aqueous phase depend on the droplet size distribution, the mixing ratio of dry aerosol particulate material to cloud droplet water, and the amount of light absorbing material in the droplets. In-droplet radical source strengths have been calculated for the most important photolytic sources of OH and SO_4^-. © 1997 Elsevier Science Ltd.

Key word index: Photolysis, photodissociation, aqueous phase, radiation transfer, cloud droplet, wet chemistry.

1. INTRODUCTION

Photolysis reactions inside cloud droplets, i.e. in the aqueous phase, initiate complex mechanisms of liquid-phase reactions which play an important role in atmospheric chemistry (e.g. Graedel and Goldberg, 1983; Lelieveld and Crutzen, 1991) and in the production of atmospheric acids and aerosol particles (e.g. Stockwell, 1994).

Like in the gaseous-phase photolysis, frequencies in the aqueous phase are calculated by integrating the actinic flux inside cloud droplets, the absorption cross-section, and the quantum yield over all wavelengths. The absorption cross-sections and quantum yields depend on the temperature and are different from their counterparts in the gaseous phase. The actinic flux inside cloud droplets can be derived from the actinic flux outside of the droplets and the optical effects of the droplets. The optical effects of the cloud droplets are determined by the droplet size distribution and the amount and optical properties of dissolved aerosol material inside the droplets. For the computation of photolysis rates, the amount of dissolved gases in the aqueous phase relative to the gas phase is relevant. Finally, the amount of gases dissolved in the liquid phase is affected by the liquid water content (lwc) of the cloud, the temperature, and the ionic activity.

In the presence of clouds, some atmospheric trace gases are dissolved to a large extent in the aqueous phase (e.g. Schwartz, 1984). Lelieveld and Crutzen (1991) show phase ratios (ratio of number of molecules in aqueous phase to number of molecules in gas phase) for gases in clouds and present a formula to determine the phase ratio. In a cloud with a liquid water content of lwc = 0.3 g m^{-3} at 268 K they found a phase ratio for HNO_3 of 1.6×10^9 and for H_2O_2 a phase ratio of 6.4. On the other hand, they also estimated phase ratios much smaller than one (e.g. the phase ratio for ozone is 1.9×10^{-7}). Temperature, cloud liquid water content, and ionic activity are controlling factors for the amount of a gaseous compound solved in the aqueous phase. Therefore,

[1] Author to whom correspondence should be addressed.

especially photolysis rates of highly soluble gases in the aqueous phase may become more important compared to their gaseous photolysis rates.

Within cloud droplets, chemical reaction rates can be enhanced compared to the gas phase (Seinfeld, 1986; Lelieveld and Crutzen, 1991) due to the possible high concentration of reactants in a relatively small volume (within a cloud droplet) and to the cage effect that water molecules exert on reactants increasing the reaction probability. On the other hand, the recombination of the products of a photodissociation process is also much more likely than in the gas phase, due to the cage effect. Therefore, the resulting quantum yields for photolysis frequencies in the aqueous phase are usually around 0.1 or even smaller (Zellner *et al.*, 1990) compared to about one for the gas phase.

Finally, the actinic flux, which describes the amount of photons available for photodissociation processes, is largely affected by the microscopic and macroscopic properties of clouds. For example, Ruggaber *et al.* (1994) calculated an increase of the actinic flux above and within the upper part of cloud layers up to a factor of 2.5 compared to the cloudless case.

Calculating the actinic flux in the presence of clouds still means neglecting many unsolved problems. On one hand, real clouds are very difficult to parameterize, due to their high temporal, vertical and horizontal variability; on the other hand most of the parameters needed to describe cloud layers are only mean values in time (e.g. hourly) and are available only locally. Usually only information about the amount of clouds, cloud base, cloud top, and cloud type is registered. Since parameters like droplet size distributions, liquid water content, phase state of the hydrometeors, and thermodynamics, and information about the aerosol particles acting as cloud condensation nuclei (CCN) are required, cloud modelling even for completely overcast situations implies a lot of simplifications.

Calculations of the photolysis frequencies in the aqueous phase are very time consuming. Therefore, in previous publications the radiation energy supply inside cloud droplets was estimated to be equal (e.g. Chameides, 1984), reduced due to reflection at the droplets surface (e.g. by 15%, Graedel and Goldberg, 1983), or enhanced due to refraction of the rays and by multiple reflections inside the droplets (e.g. by 100%, Lelieveld and Crutzen, 1991) compared to the interstitial air values. Madronich (1987) estimated that the actinic flux inside a cloud droplet can increase by a factor up to about 1.6 compared to the droplet's surrounding for the case of pure water droplets. Hough (1987) parameterized the photolysis frequencies in the aqueous phase multiplying the interstitial photolysis frequencies by an extinction coefficient for pure water.

A first step for a thorough study of the modification of the actinic flux within cloud droplets was made by Bott and Zdunkowski (1987). They used a modified Mie algorithm to calculate the flux increase within cloud droplets consisting of pure water. They found an average enhancement of more than a factor of two within droplets compared to the air surrounding the droplet. Furthermore, Bott and Zdunkowski (1987) reported that in resonance cases the flux enhancement is more than two orders of magnitude higher than the average increase. Fuller and Kreidenweis (1994) and Ray and Bhanti (1994) found resonance cases with flux increases of more than 8 and 25 orders of magnitude, respectively, for comparable conditions. They located the increase of fluxes at the droplet surface, where pure water dominates.

Real cloud droplets originate from water condensation on aerosol particles and photolysis does not take place in pure water droplets. Therefore, the influence of dissolved aerosol material on the photolysis frequencies is studied on the basis of the previous work of Bott and Zdunkowski (1987). Finally, the studies described in this paper result in a parameterization, which is applicable for chemical transport models extended to the description of the so-called "wet chemistry".

2. THEORETICAL BACKGROUND FOR ACTINIC FLUX CALCULATIONS INSIDE DROPLETS

Starting with a monochromatic plane wave of wavelength λ, travelling through an infinite homogeneous medium of inductive capacities (ε_2, μ_2) and scattered by a dielectric sphere of radius r, relative refractive index m, and inductive capacities (ε_1, μ_1), the time-averaged electromagnetic energy inside the sphere (here droplets) can be determined from Mie theory (Bott and Zdunkowski, 1987). The ratio of the electromagnetic energy density inside the droplets to the electromagnetic energy density outside the droplets will be referred to as enhancement factor. The actinic flux, essential for the determination of photolysis frequencies (Dejimerdian *et al.*, 1980) inside a droplet with radius r is determined from the absolute actinic flux outside the droplets multiplied by the calculated enhancement factor for the specific droplet. The enhancement factor is an average over the whole droplet, assuming no local effects inside the droplet, like a punctual absorber in the center of the droplet. This is consistent with the assumption that the photodissociated species are distributed over the whole droplet. Although local absorbers like soot can be present inside droplets under realistic conditions the described assumption is used as an approximation, when looking at a large droplet ensemble. Furthermore, the lack of detailed field and laboratory data makes a more detailed determination impossible. The calculated very high resonance peaks for pure water droplets do not seem to be applicable for photolysis calculations in the troposphere. Bott and Zdunkowski (1987) calculated the enhancement factor for given radii while using their modified Mie algorithm. They found enhancement factors of more than two orders

of magnitude in resonance peaks inside pure water droplets and an average enhancement factor exceeding two compared to that of a sphere of the surrounding medium with the same radius.

Since photolysis frequencies are determined by integrating the actinic flux multiplied by the absorption cross-section and quantum yield of the dissociated species over a wavelength interval (Dejimerdian *et al.*, 1980), (i) the contribution of resonance peaks to the total actinic flux and especially to the line absorption spectra of the photolysis species has to be determined for single droplets, and (ii) the effect of the droplet size distribution for different cloud types has to be taken into account. To determine the contribution of resonance peaks the most complicated case, pure water droplet, is investigated. These studies show which resolution for the wavelength and the radius grid is necessary to calculate photolysis frequencies inside droplets. Furthermore, calculations with real cloud water are of prime importance, because the imaginary part of the refractive index of real cloud water is higher than that of pure water (Andre *et al.*, 1981). Finally photolysis frequencies in the aqueous phase are calculated for realistic cloud conditions assuming typical droplet size distributions and mixing ratios of pure water mass to aerosol particle mass inside droplets for each droplet radius.

3. FLUX ENHANCEMENT INSIDE SINGLE DROPLETS

3.1. *Pure water droplet*

The Mie algorithm of Bott and Zdunkowski (1987) was used to calculate the enhancement factor for pure water droplets compared to the interstitial air. When computing the enhancement factor for different cloud droplet radii between 0.1 and 30.0 μm, resonance peaks were found for all wavelengths within the interval $280 \leqslant \lambda \leqslant 700$ nm, where the essential photolytic processes in the troposphere occur. As an example Fig. 1 shows the enhancement factors as a function of the droplet radius for 550.5 nm wavelength and pure water. The arithmetically averaged enhancement factor of 2.26 in Fig. 1 was determined by 500,000 Mie calculations with $0 < r < 10$ μm (radius increment 0.00002 μm). As well as for each fixed droplet radius (> 2 μm) resonance peaks were also found from varying the wavelength. Since the imaginary part n_i of the refractive index n of pure water is only in the order of 10^{-8} to 10^{-9} for the wavelength interval between 280 and 700 nm, resonances of higher orders occur as well. As shown in Fig. 1 the enhancement factors may be as high as several orders of magnitude in the regions of the resonance peaks. The maximum increase in Fig. 1 is 1.6×10^4, i.e. four orders of magnitude higher than the average enhancement factor of 2.26. To check whether a finer resolution for the wavelength, respectively, the droplet radius grid (i.e. taking into account more resonance peaks) yields higher photolysis frequencies the increments were reduced and the grid was red shifted/blue shifted as well. The results show that more resonance peaks were found, but the integral of the enhancement factor changed by less than 1%. Therefore, it can be concluded that the resonance peaks only little contribute to the integral. This is essential for calculations of photolysis frequencies and not all of the peaks have necessarily to be registered. Furthermore, the check showed that it is sufficient to represent each wavelength for which the extraterrestrial constant solar flux is given for STAR (Ruggaber *et al.*, 1994) by an average of 100 Mie calculations in order to obtain an error of less than 2% in the actinic flux. Therefore, for calculations of the average actinic flux enhancement inside pure water cloud droplets in the troposphere, Mie calculations at 58,500 wavelengths (280–700 nm) and for droplet radii between 0 and 30 μm with $\delta r = 0.1$ μm are sufficient. Since light absorption inside droplets due to dissolved particulate or gaseous matter reduces the resonance peaks, the error due to the possible omission of resonance peaks is smaller for realistic cloud droplets. In the following, droplets with radii $r < 1$ μm are regarded not to be activated and consequently are considered as interstitial aerosol.

3.2. *Effect of dissolved absorbers*

In contrast to pure water droplets, where no photolysis takes place in the aqueous phase, cloud droplets originate from water condensation on aerosol particles and, therefore, mostly consist of diluted aqueous solutions. The imaginary part of the refractive index, which is a measure for the radiation absorption is much higher for real cloud water than for pure water. Measurements (Andre *et al.*, 1981; Dlugi, 1996) show that the imaginary part of the refractive index n of dried bulk samples of cloud water is around 10^{-2} (Fig. 2, left axis, line with diamond symbol). In the same figure, the imaginary part of pure water is plotted (right axis, line with triangle symbol). For cloud droplets with a mixing ratio (volume aerosol material to volume pure water inside the droplet) of 1:1000, which is realistic for the smaller cloud droplets (< 10 μm), the imaginary part is around 10^{-5}. Larger cloud droplets have a mixing ratio in the order of 1:100. This results from larger aerosol particles which take up water vapor in the diffusion limited regime and therefore may even have higher imaginary parts.

Mie calculations for different mixing ratios and, therefore, different imaginary parts show (Figs 3–6) that the number and magnitude of the resonance peaks decreases with increasing imaginary part. Absorption suppresses resonances and supresses oscillations of higher orders as well. The higher the imaginary part, the lower the integrated enhancement factor and therefore the lower are the photolysis frequencies within the droplets. Figures 3–6 show the flux enhancement inside the droplet relative to the interstitial air as a function of the wavelength for different mixing ratios k. The columns in the upper left

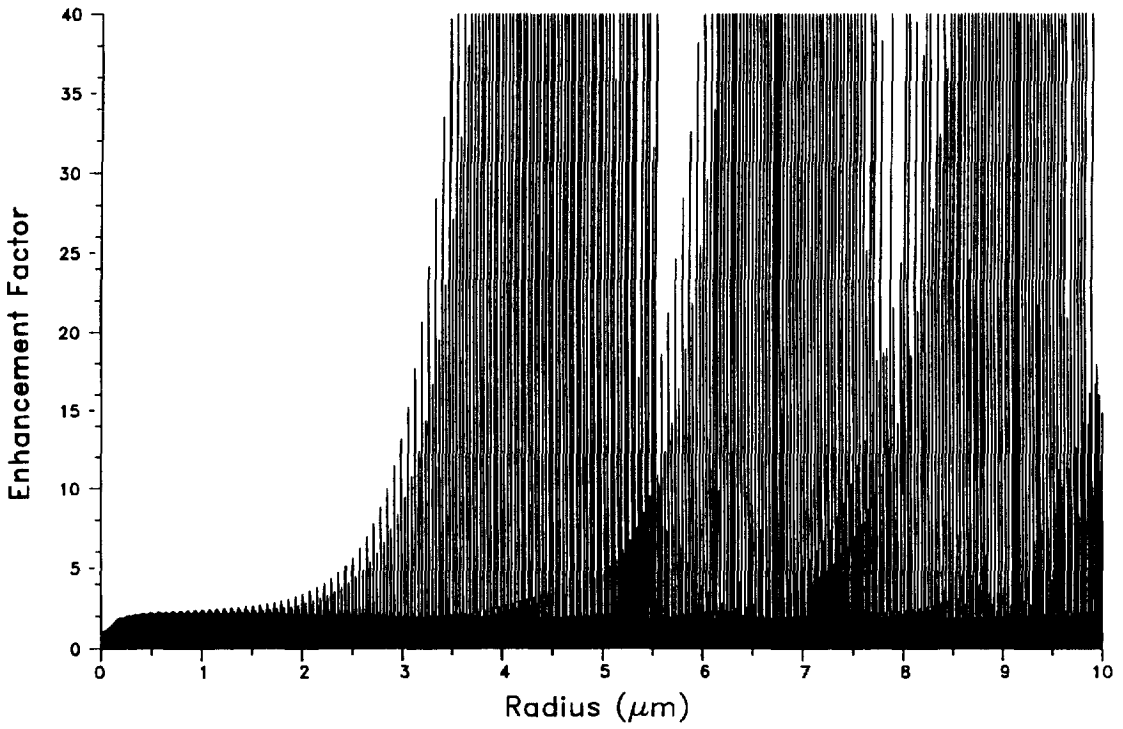

Fig. 1. Enhancement factor vs droplet radius for pure water droplet at 550.5 nm wavelength, based on 500,000 Mie calculations.

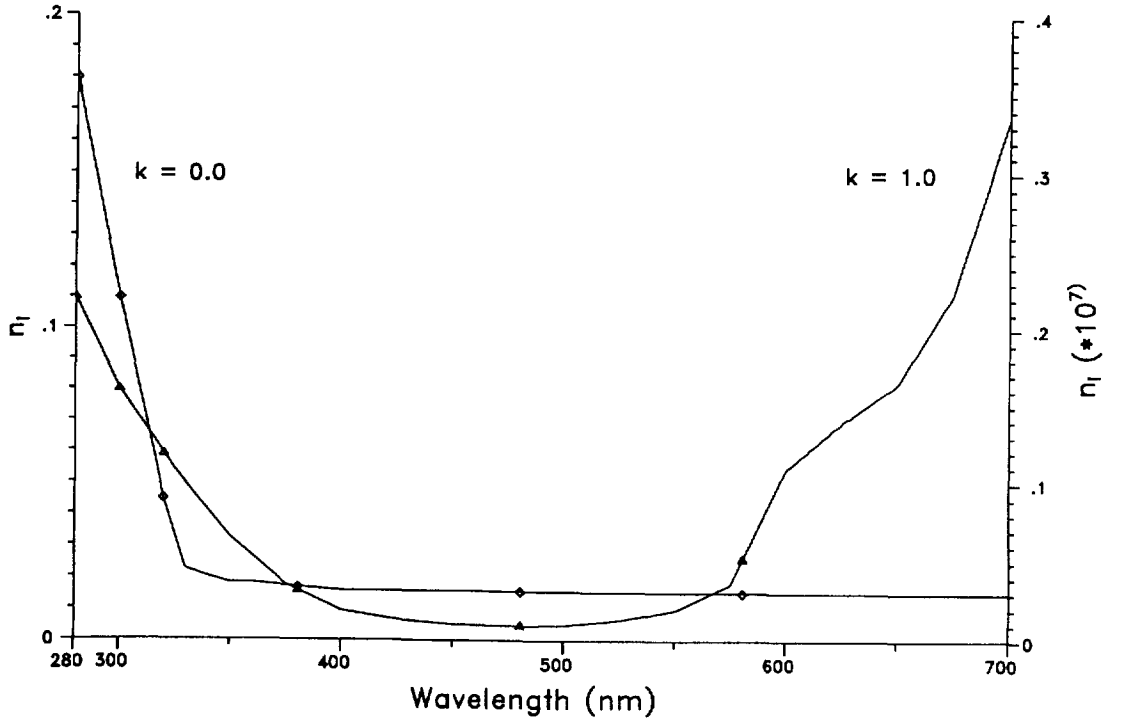

Fig. 2. Imaginary part of the refractive index vs wavelength. Left axis, curve with diamond symbol represents imaginary part of the aerosol particles ($k = 0.0$); right axis, curve with triangle symbol represents imaginary part of the refractive of pure water ($k = 1.0$).

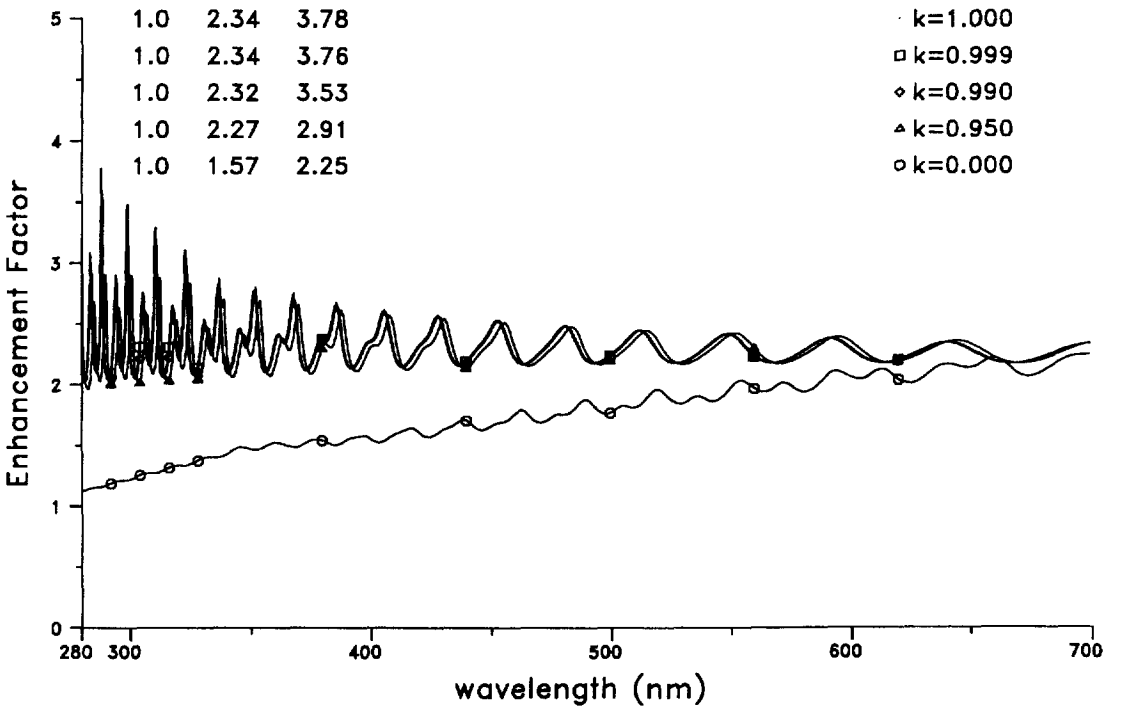

Fig. 3. Enhancement factor vs wavelength. The curves represent cloud droplets with radius $r = 1$ μm for different volume mixing ratios pure water to aerosol particles. The four columns denote from the left: droplet radius, integrated enhancement factor, maximum enhancement factor, and mixing ratio k of the imaginary part of the refractive index ($k = 1.0$ corresponds to pure water, $k = 0.0$ corresponds to pure aerosol particles).

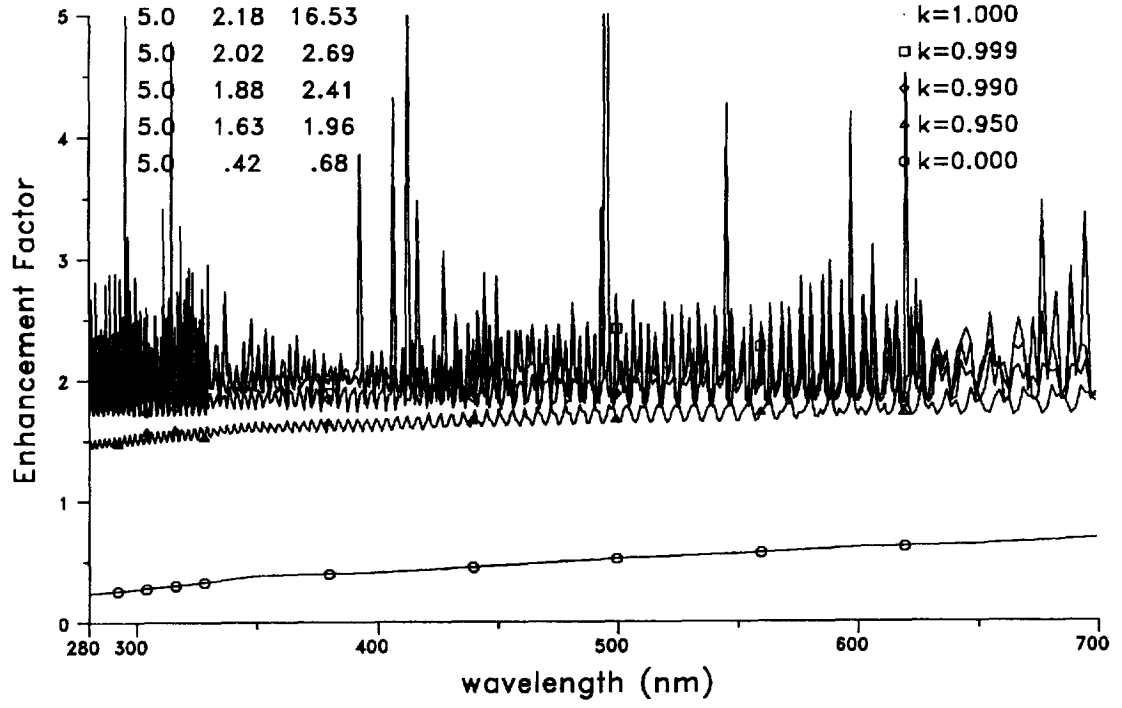

Fig. 4. As Fig. 3, but for the cloud droplet radius $r = 5$ μm.

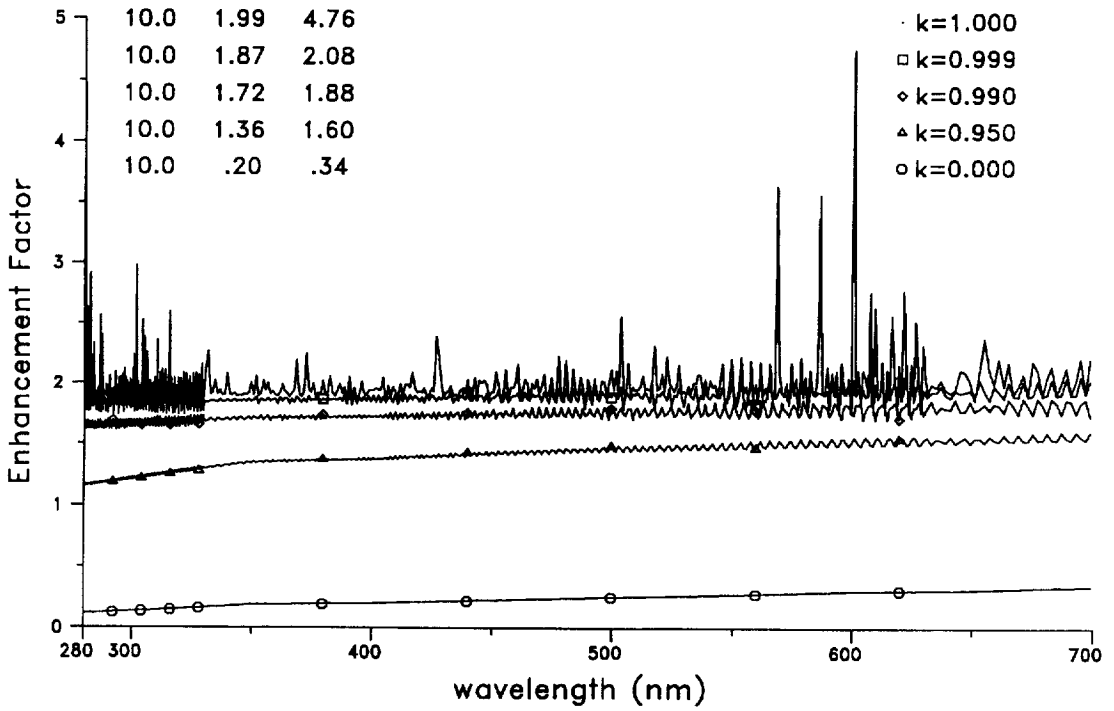

Fig. 5. As Fig. (3), but for the cloud droplet radius $r = 10\ \mu m$.

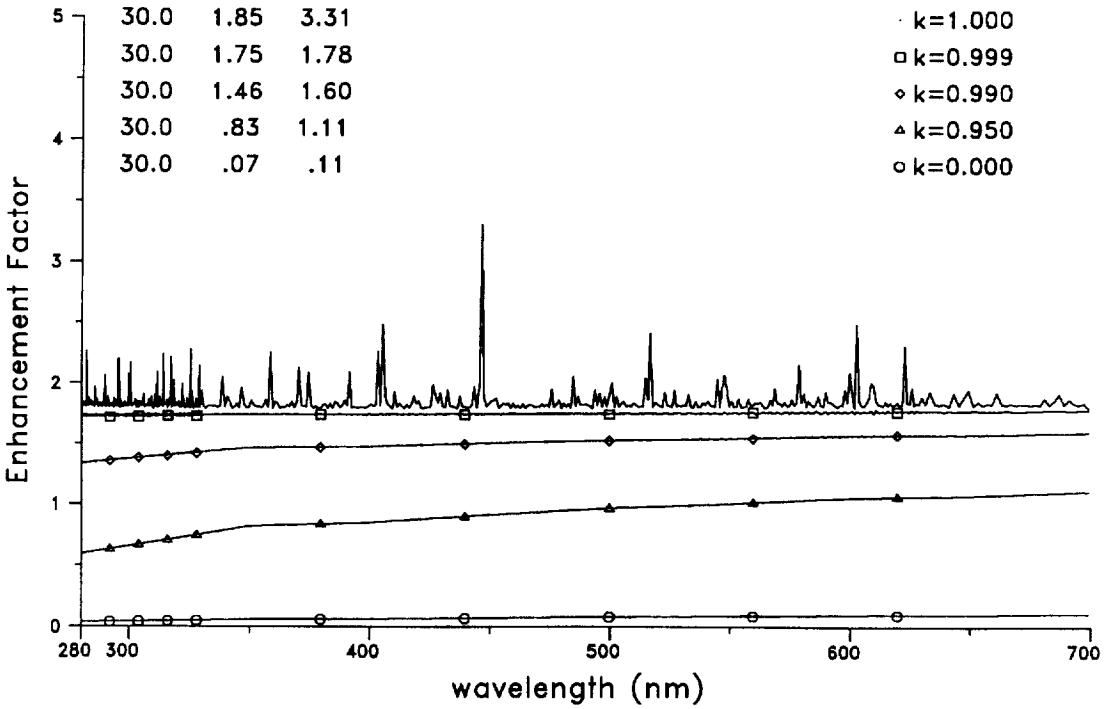

Fig. 6. As Fig. (3), but for the cloud droplet radius $r = 30\ \mu m$.

of Figs 3–6 describe (beginning from the left) the droplet radius r, the enhancement factor integrated over the relevant wavelength interval, and the maximum enhancement factor for different mixing ratios between $k = 0.0$ (dry aerosol material) and $k = 1.0$ (pure water), respectively.

As shown in Figs 3–6 for different cloud droplets radii r, the integrated enhancement factor for pure

water is reduced by increasing the mixing ratio, due to increased imaginary part of the mixture. As expected the number of resonance peaks as well as the maximum enhancement factor (3rd column) is reduced due to increasing absorption. For example, in Fig. 3 the maximum enhancement factor for pure water ($k = 1.0$) is reduced from 3.78 to 2.25 for pure aerosol particle ($k = 0.0$). Furthermore, Figs 3–6 show that the wavelength integrated enhancement factor for smaller droplets is higher than for larger droplets. Thus for droplets with radius $r > 1$ μm higher enhancement factors and therefore higher photolysis frequencies occur, compared to larger ones containing the same concentration of aerosol material. For droplet radii around 3–5 μm the highest number of resonance peaks and the highest maximum enhancement factors were found. Inside pure aerosol "droplets" ($k = 0.0$) with $r < 2$ μm enhancement factors are higher than one (Fig. 3). Inside larger droplets (Figs 3–6) the absorption strongly reduces the enhancement factor and therefore the photolysis frequencies in the pure aerosol case ($k = 0.0$). So "optimum" conditions for the enhancement of the actinic flux inside droplets must exist depending on their chemical composition.

4. FLUX ENHANCEMENT FOR DROPLET POPULATIONS

4.1. *Mixing ratios of aerosol mass to water in cloud droplets*

Water vapor condenses on aerosol particles when the air reaches supersaturation during a cooling process in the atmosphere. The evolving droplet size distribution mainly depends on the size distribution of the aerosol particles serving as cloud condensation nuclei (CCN) and the maximum supersaturation reached during cloud formation. Droplets with radii between 1 and 30 μm dominate the number concentration in most clouds.

The condensational growth of a single droplet of a given radius r, which develops at a given supersaturation on an aerosol particle with radius r_n is described by the droplet growth equation (e.g. Pruppacher and Klett, 1978, equations (13)–(28)). The growth of the droplets is limited by the diffusion of water vapor. Within a given droplet population, the droplets compete for the available water vapor. Therefore, the mixing ratio of water to dissolved material of the CCN itself depends on the time-dependent droplet size. To obtain the mixing ratio of cloud water and dissolved aerosol material of the droplet size, the droplet growth equation was solved starting with different aerosol size distributions, which can be regarded as typical for rural, urban, and maritime conditions (Bott, 1991; Hess *et al.*, 1996). As an example, Fig. 7 shows a computed droplet size distribution and volume mixing ratio of aerosol material to water in cloud droplets for the aerosol type "Average Continental" of Hess *et al.* (1996). The liquid water content is $0.14\,g\,m^{-3}$. Since the actinic flux for particles with $r \leqslant 0.1$ μm is small (Fig. 1), only the

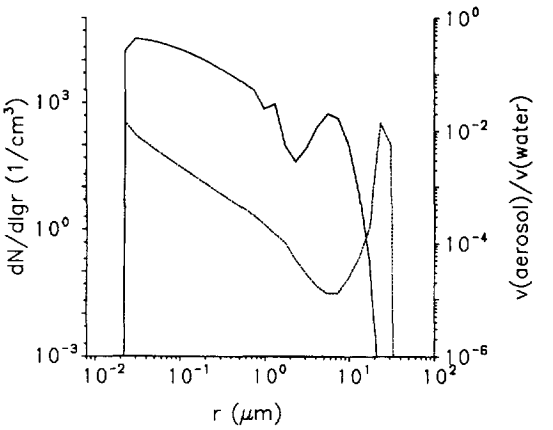

Fig. 7. Computed droplet size distribution (——) and volume mixing ratio of aerosol material to water in cloud droplets (– – –) for a continental aerosol size distribution.

growing droplets to the right of the minimum of the droplet size distribution contribute to the actinic flux. For these droplets the mixing ratio between water and aerosol material is on the order of 10^{-4} with slightly higher values for the larger droplets. These mixing ratios agree with estimations based on the measured data from Andre *et al.* (1981) and Dlugi (1996).

4.2. *Size distribution of cloud droplets*

For the purpose of modelling cloud effects on radiative transfer, different cloud types are usually described by standard droplet size distributions (Tampieri and Tomasi, 1976), as shown in Fig. 8. Since these size distributions are frequently used, the growing droplet modes of computed size distributions were represented by these distributions. To calculate, for example, the enhancement factor of a cumulus cloud the spectral enhancement factors for a specific mixing ratio and for each droplet radius have to be integrated over all radii, taking into account the droplet size distribution. In this way the spectral enhancement factors for the different cloud types can be determined using different droplet size distributions. Figures 9 and 10 compared with Fig. 8 show conditions obtained for the "rural" aerosol (Bott, 1991) acting as CCN. The smaller the droplets in a cloud are, the higher are the enhancement factors and therefore the photolysis frequencies. Figures 11, 12 show the same results as Figs 9, 10, respectively, but for the originate aerosol type "Average Continental" (Hess *et al.*, 1996). Therefore, the originating aerosol type has small influence on the enhancement factors and, consequently, on the photolysis frequencies in the aqueous phase in the case of mature clouds.

5. PHOTOLYSIS FREQUENCIES AND RADICAL SOURCE STRENGTHS INSIDE DROPLETS

A number of photochemical redox reactions are collected by Weschler *et al.* (1986), Graedel *et al.* (1983)

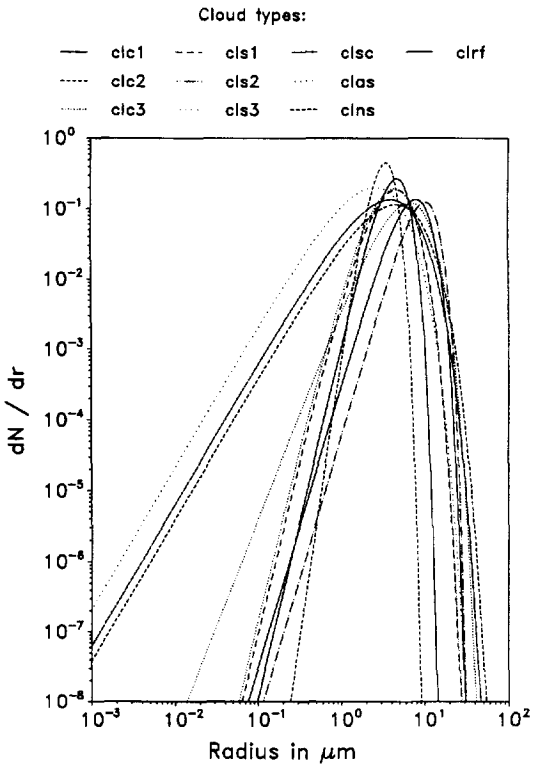

Fig. 8. Typical cloud droplet spectra for different cloud types (Tampieri and Tomasi, 1976).

and Faust (1994). Several species undergoing photolysis serve as sources for OH radicals.

Photolysis frequencies in the aqueous phase are calculated by integrating the spectral actinic flux for interstitial air multiplied by the enhancement factor, the absorption cross-sections, and the quantum yields over all wavelengths. The enhancement factor depends on the wavelength, the mixing ratio of aerosol particle to pure water, and the cloud droplet radius. Size distributions for different cloud types are used to parameterize the actinic flux enhancement in the aqueous phase for cloud droplet populations.

The absorption cross-sections and quantum yields of the photolytic reactions in the aqueous phase are determined from measurements and are different from their counterparts in the gaseous phase. The most essential photolysis reactions in the aqueous phase (e.g. Faust, 1994), which were taken into account in the present work are:

$$H_2O_2 + h\nu \rightarrow 2OH$$

$$NO_2^- + H^+ + h\nu \rightarrow NO + OH$$

$$NO_3^- + H^+ + h\nu \rightarrow NO_2 + OH$$

$$[Fe^{III}(OH)]^{2+} + h\nu \rightarrow Fe^{II} + OH$$

$$[Fe^{III}(OH)_2]^+ + H^+ + h\nu \rightarrow Fe^{II} + OH + H_2O$$

$$[Fe^{III}(SO_4)]^+ + h\nu \rightarrow Fe^{II} + SO_4^-.$$

The absorption cross-sections and quantum yields are taken from Zellner *et al.* (1990) and references therein for the absorption cross-sections and quantum yields of OH formation in the photolysis of nitrate, nitrite, and hydrogen peroxide. The corresponding data for the photolysis of $[Fe(OH)]^{2+}$ were taken from Benkelberg *et al.* (1991) and Faust and Hoigné (1990). Data for the absorption coefficients of $[Fe(OH)_2]^+$ were taken from Weschler *et al.* (1986), whereas the quantum yield of OH formation of this complex is again taken from the study by Benkelberg *et al.* (1991). The photochemical data for the photolysis of the $[Fe(SO_4)]^+$ complex were taken from Benkelberg and Warneck (1995).

As examples Figs 13 and 14 show the calculated photolysis frequencies of nitrate, nitrite, and hydrogen peroxide together with the corresponding gaseous-phase photolysis frequencies and the photolysis frequencies of the iron complex in the aqueous phase. For the present studies, the calculations were done with STAR (Ruggaber *et al.*, 1994). These case studies were done with the U.S. Standard profiles with a total column ozone content of 300 DU (= 0.3 atm cm) and a total aerosol optical depth of 0.2 for 500 nm wavelength as input. A cloud with a lwc of 0.3 g m^{-3} for Fig. 13 and a lwc of 0.0125 g m^{-3} for Fig. 14 and the droplet size distribution "cul" (Fig. 8) from 1 up to 5 km height above surface was assumed to be present. The optical thickness at 500 nm wavelength of the cloud is 398.4 and 16.6 in the cases of Figs 13 and 14, respectively. The first cloud case is a optically thick culumus cloud; the second is the climatological average cloud for central Europe. The solar zenith angle is 60° and the surface albedo of grassland was applied. The maximum values of the photolysis frequencies are obtained in the top part of the cloud. With decreasing height the photolysis frequencies decrease in the cloud.

Radical source strengths were calculated for the first cloud case, using the obtained photolysis frequencies and the concentrations for the radical precursors as shown in Table 1 together with the corresponding references. For the second case, the values are slightly smaller in the upper part of the cloud, but larger in the lower part of the cloud compared with the first cloud case as the comparison of Fig. 13 with Fig. 14 shows. The results for two different lwc's and a zenith angle of 60° are shown in Table 2. The solar zenith angle of 60° represents average daily conditions for midlatidudes. From these results several conclusions can be drawn. It can be seen that a radical-driven droplet photochemistry is expected to be most efficient at the cloud top. Generally, source strengths (as well as photolysis frequencies) are by one order of magnitude higher at the cloud top than at the base of a optical thick cloud. With regard to the different chemical system studies it is obvious that the contribution of the photolysis of the Fe(III)-sulfato complex only leads to a small source strength for the photochemical formation of sulfate radical anions when compared to the OH

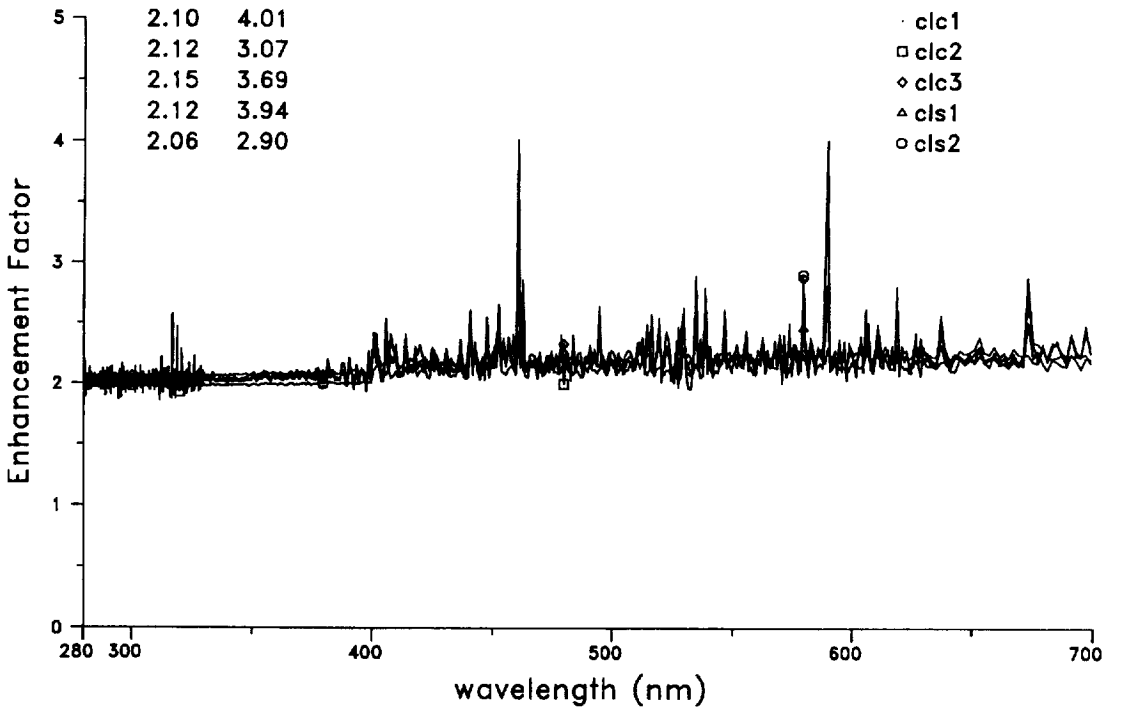

Fig. 9. Enhancement factor vs wavelength integrated over the radius taking into account different droplet size distributions. Originate aerosol: rural.

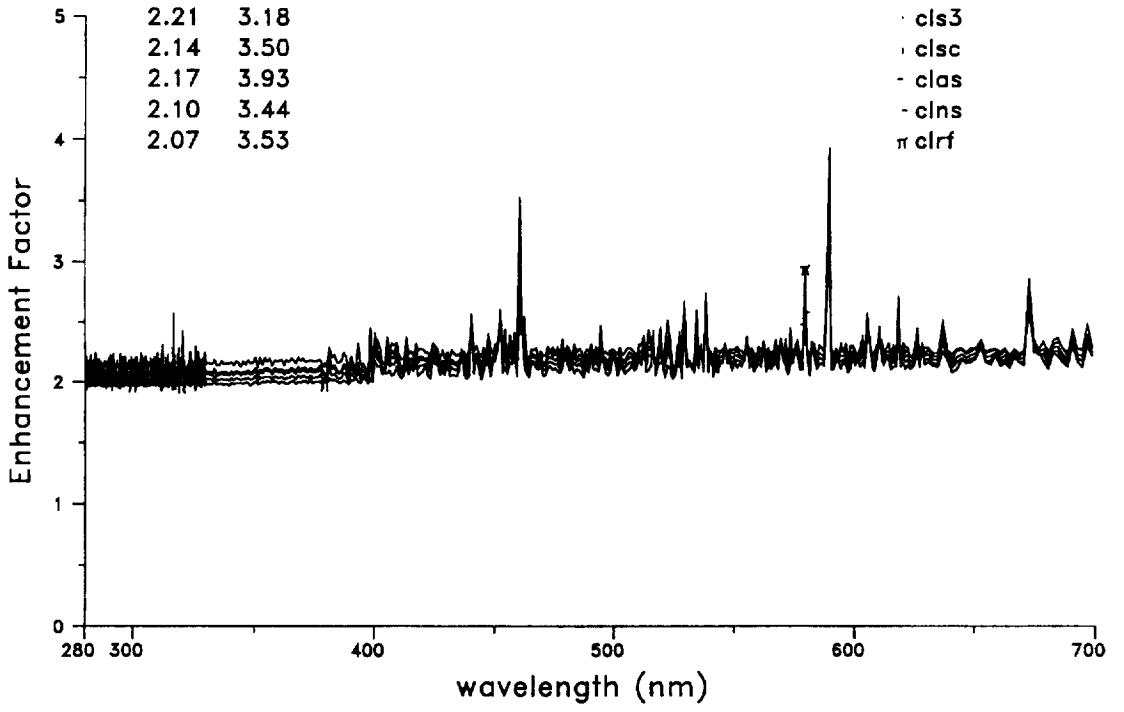

Fig. 10. Enhancement factor vs wavelength integrated over the radius taking into account different droplet size distributions. Originate aerosol: rural.

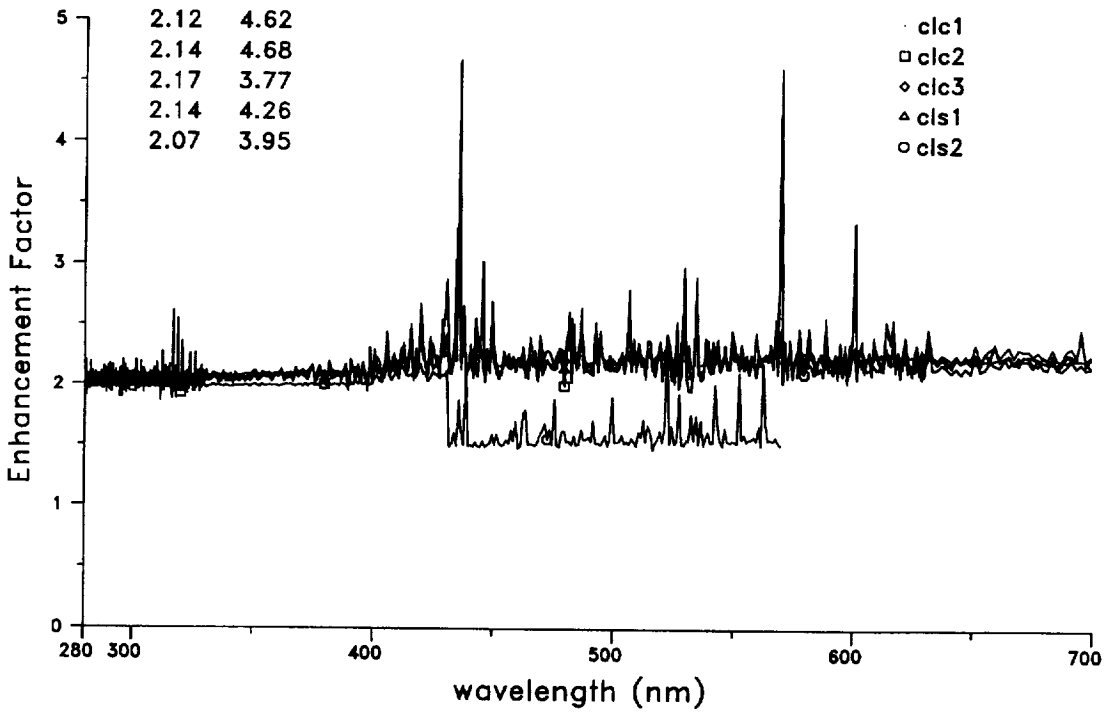

Fig. 11. Enhancement factor vs wavelength integrated over the radius taking into account different droplet size distributions. Originate aerosol: average continental.

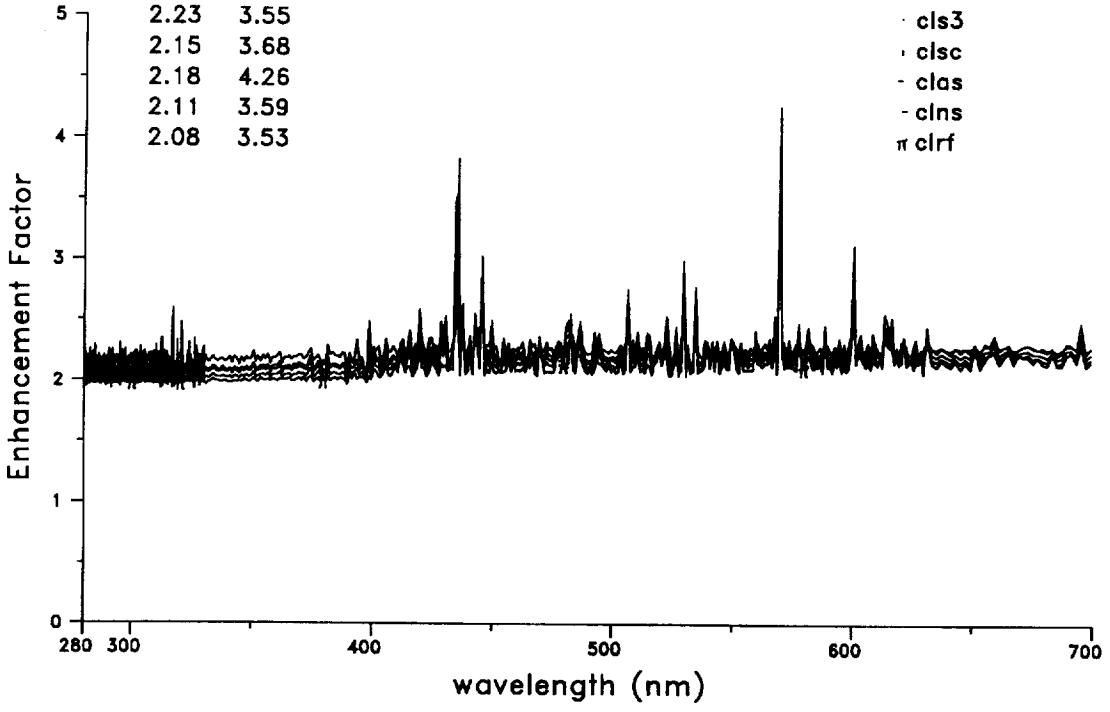

Fig. 12. Enhancement factor vs wavelength integrated over the radius taking into account different droplet size distributions. Originate aerosol: average continental.

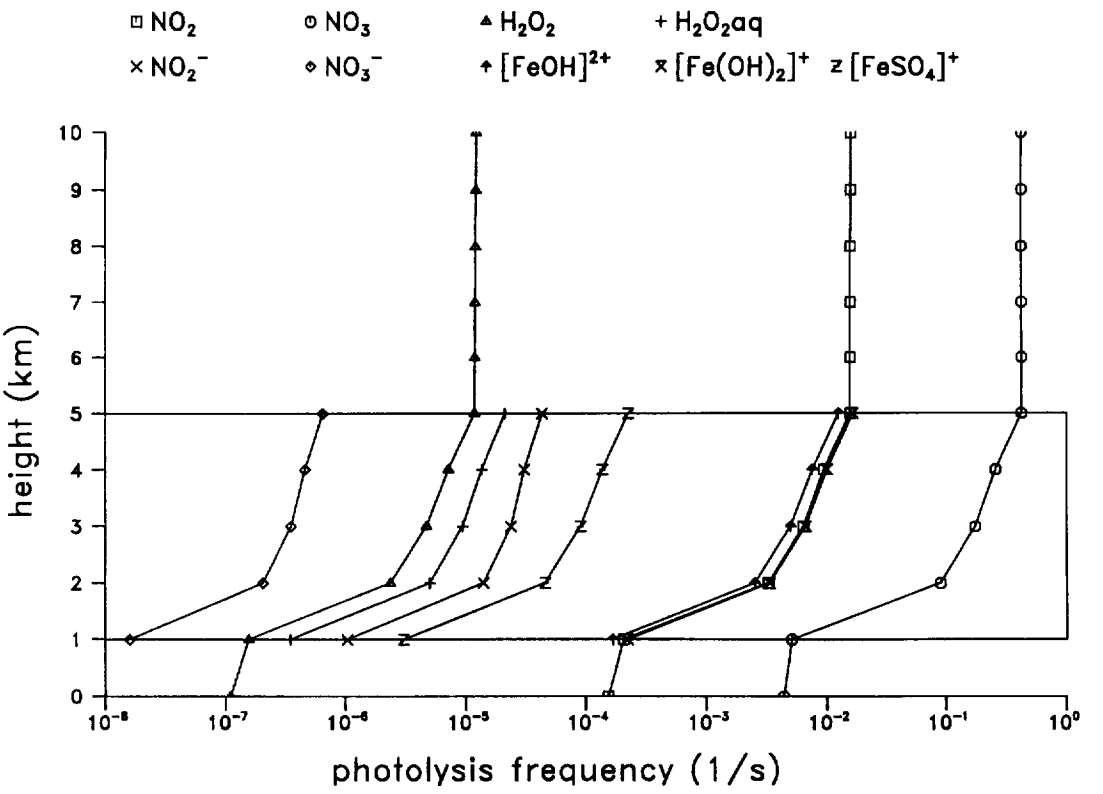

Fig. 13. Photolysis frequencies in the aqueous phase and gaseous phase vs height for the U.S. standard atmosphere and a solar zenith angle of 60°. Cloud base: 1 km, cloud top: 5 km, lwc = 0.3 g m^{-3}.

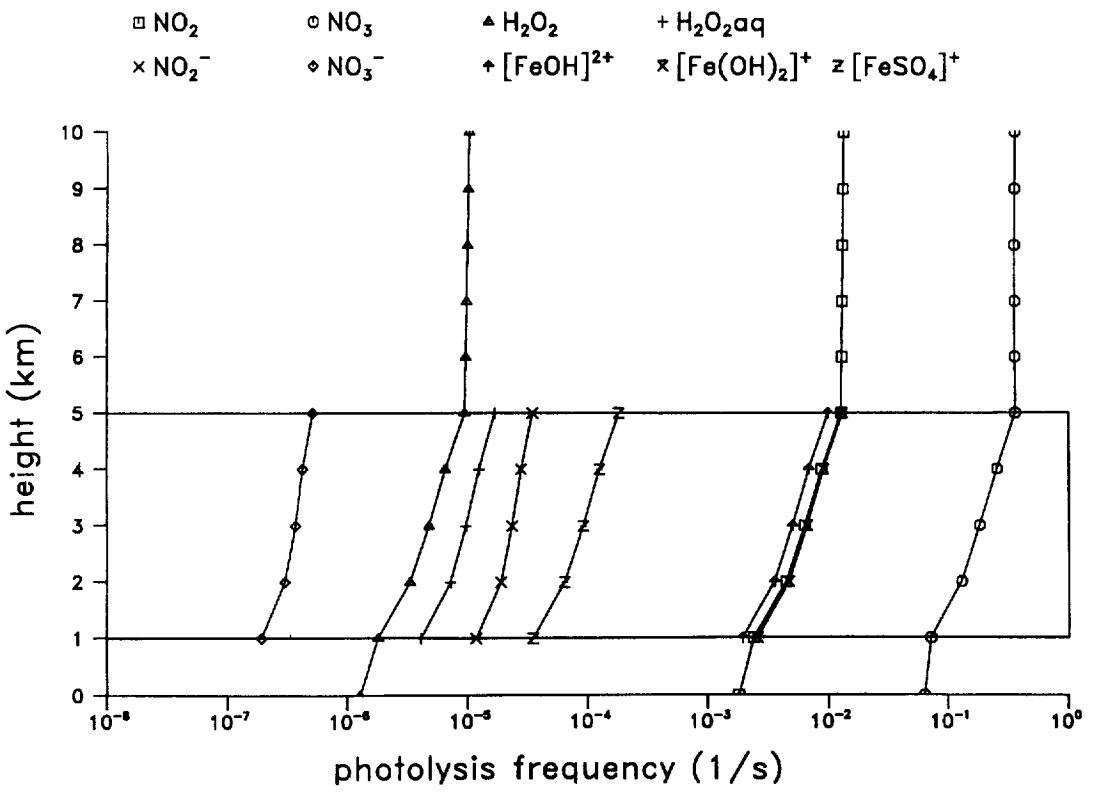

Fig. 14. As Fig. (13), but for lwc = 0.0125 g m^{-3}.

Table 1. Cloud water concentrations of aqueous phase radical precursors

Species	Typical concentration ($mol\,\ell^{-1}$)	Reference
H_2O_2	3.0×10^{-5}	Warneck (1992)
NO_2^-	2.6×10^{-7}	Zellner *et al.* (1990)
NO_3^-	2.5×10^{-5}	Zellner *et al.* (1990)
$[Fe^{III}(OH)]^{2+}$	2.5×10^{-7}	Estimated (1)
$[Fe^{III}(OH)_2]^+$	2.5×10^{-7}	Estimated (1)
$[Fe^{III}(SO_4)]^+$	1.0×10^{-8}	Estimated (2)

Note: (1) Own estimate: total concentration of iron(III) is estimated as $[Fe(III)]_{tot} = 2 \times 10^{-6}\ mol\,\ell^{-1}$, after Warneck (1992). Twenty five percent are supposed to exist in soluble form and the concentrations of both complexes are estimated to be equal for the two complexes.

(2) Own estimate, the concentration of this complex is highly dependent on pH and sulfate concentration.

systems. Nevertheless, this process may not be unimportant when its source strength is compared to other sulfate radical formation processes, especially in the radical-driven oxidation of sulfur(IV). Regarding the photochemical OH-formation processes, the most efficient radical sources are found to be the photolysis reactions of the Fe(III)-hydroxy complexes. Obviously, the exact speciation of these complexes is not critical in assessing their relative contributions to OH formation. The concentrations of the iron(III) complexes, however, are hard to access and further experiments are needed to obtain more reliable input parameters for detailed modelling studies. From the remaining OH sources clearly hydrogen peroxide photolysis is the dominant OH source which, however, may only account for OH fluxes smaller than those from the iron complexes by about one order of magnitude. Hydrogen peroxide photolysis may serve as a photochemical OH source in cloud droplets where little dissolved iron(III) is available. If the concentrations of Table 1 are applied, the photolysis of nitrate and nitrite anions are even much weaker OH sources than hydrogen peroxide photolysis.

6. ESTIMATION OF AQUEOUS PHASE ABSORPTION

To estimate whether absorption processes involved in photodissociation in the aqueous phase have effects on radiation fluxes or not, the absorption coefficients of photolysed species are compared with the extinction coefficients of the cloud droplets and the interstitial aerosol and air. To determine the absorption coefficient the concentration of a photolysed species in the cloud water has to be multiplied by the absorption cross-section, and the ratio of the droplet volume to the volume of droplet and interstitial air. In the case of NO_3^- the typical concentration is $2.5 \times 10^{-5}\ mol\,\ell^{-1}$ and the absorption cross-section is around $2 \times 10^{-20}\ cm^2$. Therefore the absorption coefficient inside the droplet is 6.022045×10^{23} (molecules mol^{-1}) $\times 2.5 \times 10^{-8}$ ($mol\ cm^{-3}$) $\times 2 \times 10^{-20}$ (cm^2) = 30 (km^{-1}). Assuming an average droplet radius of 10 μm and 500 droplets cm^{-3} the volume absorption coefficient of NO_3^- is 6×10^{-5} (km^{-1}). The absorption coefficient for the other species shown in Table 1 is lower than for that for NO_3^-. The comparison of this absorption coefficient with the orders of magnitude of the coefficients of molecular scattering (10^{-1} (km^{-1})), aerosol extinction (10^{-1} (km^{-1})), gas absorption (10^{-1} (km^{-1})) and droplet extinction (10^2 (km^{-1})) in the lower troposphere shows, that the absorption due to photolytic processes has minor effect on radiation quantities. However, local absorbers like soot as found in realistic cloud water reduce significantly all radiation quantities compared to calculations with pure water.

7. CONCLUSIONS

To calculate photolysis frequencies in the aqueous phase a parameterization was developed, with which the actinic flux inside cloud droplets can be derived from the actinic flux outside the droplets. On the basis of rigorous Mie theory taking into account the effect of dissolved particulate aerosol material the enhancement factors of the actinic flux inside cloud droplets to

Table 2. Calculated radical source strengths ($mol\,\ell^{-1}\,s^{-1}$) for OH (columns 1–5) and SO_4^- (column 6) within cloud droplet precursors, according to Fig. 13

Height (km)	H_2O_2	NO_2^-	NO_3^-	$[Fe^{III}(OH)]^{2+}$	$[Fe^{III}(OH)_2]^+$	$[Fe^{III}(SO_4)]^+$
(a) *lwc* = 0.1 $g\,m^{-3}$, zenith angle 60°						
4	4.0×10^{-10}	7.7×10^{-12}	1.1×10^{-11}	1.9×10^{-9}	2.5×10^{-9}	1.3×10^{-12}
3	2.9×10^{-10}	6.1×10^{-12}	9.2×10^{-12}	1.3×10^{-9}	1.7×10^{-9}	9.2×10^{-13}
2	1.7×10^{-10}	3.9×10^{-12}	5.8×10^{-12}	6.9×10^{-10}	9.1×10^{-10}	5.0×10^{-13}
1	2.9×10^{-11}	7.1×10^{-13}	1.1×10^{-12}	1.1×10^{-10}	1.5×10^{-10}	8.2×10^{-14}
(b) lwc = 0.3 $g\,m^3$, zenith angle 60°						
4	4.0×10^{-10}	7.9×10^{-12}	1.1×10^{-11}	1.9×10^{-9}	2.5×10^{-9}	1.4×10^{-12}
3	6.9×10^{-10}	6.1×10^{-12}	8.8×10^{-12}	1.2×10^{-9}	1.7×10^{-9}	9.0×10^{-13}
2	1.5×10^{-10}	3.6×10^{-12}	5.1×10^{-12}	6.3×10^{-10}	8.3×10^{-10}	4.5×10^{-13}
1	9.8×10^{-12}	2.5×10^{-13}	3.7×10^{-13}	3.9×10^{-11}	5.2×10^{-11}	2.9×10^{-14}

the actinic flux outside the droplets were determined for wavelengths between 280 and 700 nm for 10 predefined droplet size distributions. The input parameters for the parameterization are the mixing ratio of aerosol material to pure water and the refractive index of the aerosol material. The actinic flux inside the droplets can be derived by multiplication of the actinic flux outside the droplets with these enhancement factors. Now photolysis frequencies in the aqueous phase can be computed by integrating the actinic flux inside cloud droplets, the absorption cross-section, and the quantum yield over all wavelengths. The parameterization is independent of the radiation transfer model and the enhancement factors are available on discette on request.

Studies are performed to find the essential parameters and to show the effects on the photolysis frequencies in the aqueous phase and the radical source strengths. The results show that the actinic flux inside cloud droplets are on the average more than twice as large as compared to the interstitial air. To determine the photolysis frequencies in the aqueous phase accurately, the knowledge of the size distribution of the cloud droplets, the optical depth of the cloud and the refractive index for each droplet size is essential. Using the refractive index of pure water instead of a realistic refractive index, taking into account dissolved aerosol material, overestimates the radiation quantities inside droplets by an average of 20%. Variations of the aerosol type have small influence on the photolysis frequencies in the aqueous phase. But as higher the portion of absorbing material of the originate aerosol particle is, as lower the photolysis frequencies in the aqueous phase are. Resonance peaks which could be found for each wavelength or each droplet radius contribute only little to the integral. Due to optical effects the enhancement factors and therefore the radiation quantities inside smaller droplets are higher than in larger droplets for the same aerosol concentration. The absorption processes of photolysed species have minor effect on radiation quantities outside the cloud droplets.

Radical-driven droplet photochemistry is most efficient at the cloud top. Generally, source strengths (as well as photolysis frequencies) are one order of magnitude higher at cloud top compared to the base of a optical thick cloud. With regard to the photochemical OH-formation processes, the most efficient radical sources are found to be the photolysis reactions of the Fe(III)-hydroxy complexes. If dissolved iron(III) is not available hydrogen peroxide photolysis may serve as an photochemical OH source in cloud droplets.

These studies are based on the assumption that all absorbers are evenly distributed within the cloud droplets and that the cloud droplets are spherical. Soot particles adsorbed on the surface (= outside) of the cloud droplet or existing as a nucleus in a water cage are not covered by these assumptions. Compared to equally distributed absorbers such local absorbers may have no effect on the radiation due to optical refraction at the droplet surface, as well as an increasing influence due to focusing by optical refraction. This assumption is the limiting factor of this parameterization.

Acknowledgements—This study was performed within the EUROTRAC-subprojects EUMAC and HALIPP. Many thanks to W. Seidl for his support and useful comments. We gratefully acknowledge support by the Bundesministerium fur Bildung und Wissenschaft, Forschung und Technologie (BMBF) for two of the authors (AR, RF) under Contract No. 521-4007-07EU738 8 (EUMAC) and two of the authors (HH, H-WJ) under Contract No. 521-4007-07EU780A1.

REFERENCES

Andre, K., Dlugi, R. and Schnatz, G. (1981) Absorption of visible radiation by atmospheric particles, fog and cloud water residues. *J. Atmos. Sci.* **38**, 141–155.

Benkelberg, H. J., Schäfer, A. and Warneck, P. (1991) *Air Pollution Research Report* 33: *Atmospheric Oxidation Processes*, ed. K. H- Becker, CEC, Brussels, p. 130.

Benkelberg, H. J. and Warneck, P. (1995) Photodecomposition of Iron(III) hydroxo and sulfato complexes in aqueous solution: wavelength dependence of OH and SO4- quantum yields. *J. Phys. Chem.* **99**, 5214.

Bott, A. (1991) On the influence of the physico-chemical properties of aerosols on the life cycle of radiation fogs. *Boundary Layer Met.* **56**, 1–31.

Bott, A., and Zdunkowski, W. (1987) Electromagnetic energy within dielectric spheres. *J. Opt. Soc. Am. A* **4**, 1361–1365.

Chameides, W. L. (1984) The photochemistry of a remote marine stratiform cloud. *J. Geophys. Res.* **89**, 4739–4755.

Demerjian, K. L., Schere, K. L. and Peterson, J. T. (1980) Theoretical estimates of actinic (spherically integrated) flux and photolytic rate constants of atmospheric species in the lower troposphere. *Adv. Envir. Sci. Technol.* **10**, 369–459.

Dlugi R. (1996) unpublished results.

Faust, B. C., (1994) A review of the photochemical redox reactions of Iron(III) species in atmospheric, oceanic, and surface waters: influences on geochemical cycles and oxidant formation. In *Aquatic and Surface Photochemistry*, eds. G. R. Helz, R. G. Zepp and D. G. Crosby, pp. 3–37. Lewis, Ann Arbor.

Faust, B. C. and Hoigné, J. (1990) Photolysis of Fe(III)-hydroxy complexes as sources of OH radicals in clouds, fog, and rain. *Atmospheric Environment* **24A**, 79.

Fuller, K. A., and Kreidenweis, S. M. (1994) Contributions of morphology dependent resonances to the actinic flux inside cloud droplets. In *Fourth International Aerosol Conference* 29.8.–2.9.1994, *Abstracts*, ed. R. C. Flagan, p. 475.

Graedel, T. E., and Goldberg, K. I. (1983) Kinetic studies of raindrop chemistry. 1. Inorganic and organic processes. *J. Geophys. Res.* **88**, 10865–10882.

Hess, M., Koepke, P. and Schult, I. (1996) Optical properties of aerosols and clouds: The software package OPAC. *J. Atmos. Ocean. Techn.*, submitted.

Hough, A. M. (1987) A computer modelling study of the chemistry occurring during cloud formation over hills. *Atmospheric Environment* **21**, 1073–1095.

Lelieveld, J., and Crutzen, P. J. (1991) The role of clouds in tropospheric photochemistry. *J. Atmos. Chem.* **12**, 229–267.

Madronich, S. (1987) Photodissociation in the atmosphere, 1, Actinic flux and the effects of ground reflections and clouds. *J. Geophys. Res.* **92** (D8), 9740–9752.

Pruppacher, H. R. and Klett, J. D. (1978) *Microphysics of Cloud and Precipitation*. D. Reidel, Doordrecht.

Ray, A. K. and Bhanti, D. (1994) Photochemical reactions in microdroplets: effects of resonances. In *Fourth International Aerosol Conference* 29.8.–2.9.1994, *Abstracts*, ed. R. C. Flagan, p. 476.

Ruggaber, A., Dlugi, R. and Nakajima, T. (1994) Modelling of radiation quantities and photolysis frequencies in the troposphere. *J. Atmos. Chem.* **18**, 170–210.

Schwartz, S. E. (1984) Gas-aqueous reactions of sulfur and nitrogen oxides in liquid-water clouds. In *SO_2, NO and NO_2 Oxidation Mechanisms: Atmospheric Considerations*, ed. J. G. Calvert, Vol. 3, Acid Precipitation Series. Butterworth, Boston, 173–208.

Seinfeld, J. H. (1986) *Atmospheric Chemistry and Physics of Air Pollution*. Wiley, New York.

Stockwell, W. R. (1994) The effect of gas-phase chemistry on aqueous-phase sulfur dioxide oxidation rates. *J. Atmos. Chem.* **19**, 317–329.

Tampieri, F. and Tomasi, C. (1976) Size distribution models of fog and cloud droplets in terms of modified gamma function. *Tellus* **28**, 333–347.

Warneck, P. (1992) Chemistry and photochemistry in atmospheric water droplets. *Ber. Bunsenges. Phys. Chem.* **96**, 454.

Weschler, C. J., Mandich, M. L. and Graedel, T. E. (1986) Speciation, photosensitivity, and reactions of transition metal ions in atmospheric droplets, *J. Geophys. Res.* **91**, 5189–5204.

Zellner, R., Exner, M. and Herrmann, H. (1990) Absolute OH quantum yields in the laser photolysis of nitrate, nitrite and dissolved H_2O_2 at 308 and 351 nm in the temperature range 278–353 K. *J. Atmos. Chem.* **10**, 411–425.